# *Small-amplitude acoustics in bulk granular media*

# Small-amplitude acoustics in bulk granular media

David L. Henann,[1,*] John J. Valenza, II,[2] David L. Johnson,[2] and Ken Kamrin[1]
[1]*Department of Mechanical Engineering, MIT, Cambridge, Massachusetts 02139, USA*
[2]*Sensor Physics, Schlumberger-Doll Research, Cambridge, Massachusetts 02139, USA*
(Received 3 August 2013; revised manuscript received 8 October 2013; published 31 October 2013)

We propose and validate a three-dimensional continuum modeling approach that predicts small-amplitude acoustic behavior of dense-packed granular media. The model is obtained through a joint experimental and finite-element study focused on the benchmark example of a vibrated container of grains. Using a three-parameter linear viscoelastic constitutive relation, our continuum model is shown to quantitatively predict the effective mass spectra in this geometry, even as geometric parameters for the environment are varied. Further, the model's predictions for the surface displacement field are validated mode-by-mode against experiment. A primary observation is the importance of the boundary condition between grains and the quasirigid walls.

DOI: 10.1103/PhysRevE.88.042205 PACS number(s): 45.70.−n, 83.10.Ff, 43.20.Gp, 43.20.Jr

## I. INTRODUCTION

The propagation of small-amplitude elastic waves through granular media is central to a variety of phenomena. For example, carefully designed granular crystals can exhibit frequency band gaps or be designed as waveguides [1–3]. Alternatively, many industries, such as automotive, aerospace, and oil and gas, are interested in utilizing bulk granular media—a large amorphous collection of densely packed grains—to attenuate, or damp, elastic waves [4–8]. Modeling techniques are crucial for the design and optimization of devices involving granular acoustics. Due to the periodic arrangement of grains, discrete methods are appropriate for modeling wave propagation in granular crystals; however, continuum methods are desired to model bulk granular media due to the large number of grains and amorphous structure. Continuum modeling of wave propagation in bulk granular materials has remained an open modeling issue. In particular, the importance of material nonlinearity due to the Hertzian nature of the intergranular contacts is not clear (see [9,10]), nor is it clear to what extent complex grain-wall interactions may be simplified within a model.

As a straightforward example, we consider the benchmark problem of a shaker cup filled with grains under one-dimensional excitation, pictured schematically in Fig. 1. The cup is subjected to a broad range of frequencies, and at each frequency, $f$, the complex-valued acceleration of the cup, $\tilde{a}(f)$, and the force exerted upon the cup, $\tilde{F}(f)$, may be measured. The effective mass of the granular media is then defined as

$$\tilde{M}(f) = \frac{\tilde{F}(f)}{\tilde{a}(f)} - M_{\mathrm{C}}, \tag{1}$$

where $M_{\mathrm{C}}$ is the (real-valued) static mass of the cup. On a macroscopic scale, the dynamic effective mass is useful for understanding the frequency-dependent acoustic properties and dissipative capacity of the granular system. A notable observation from experiments is that resonant peaks do not occur at ratios of $1:3:5:7:\ldots$, as would be expected for the one-dimensional vibration of a linear elastic solid, and the relative importance of material nonlinearity and boundary effects in determining the ratio of resonant peaks is not clear. Therefore, in this paper, we propose a general method for modeling small-amplitude bulk granular acoustics and validate that it produces quantitative predictions of experimental measurements in this benchmark case.

## II. EXPERIMENTAL METHODS AND RESULTS

We consider fine-grained ($\sim 10^{-1}$ mm) tungsten (W) particles with irregular grain shape, described in [11]. Effective mass measurements were conducted using the cylindrical cup apparatus shown schematically in Fig. 1, with a diameter of $2R = 25.4$ mm. The filling depth, $L$, of the granular media was varied to test the effect of the aspect ratio, $R/L$. Prior to the measurement of $\tilde{M}(f)$, the tungsten grains were coated with a thin ($\ll$ grain size) layer of polydimethylsiloxane (PDMS), using the process reported in [12]. The result of this process is a thin, solid viscoelastic film on each grain, which increases the damping capacity of the grains, as is desired in industrial applications. The dry, coated grains were then poured into the cup and subjected to a stress-controlled mechanical compaction protocol, described extensively in [11], to achieve some degree of consolidation.

### A. Effective mass measurement

The complex-valued effective mass of the granular media $\tilde{M}(f)$ was then experimentally measured for different aspect ratios, $R/L$, in the following manner. After employing the consolidation protocol, the cup was affixed to the top of a force gauge, which in turn was affixed to a minishaker. Two accelerometers were glued to the bottom of the cup, at opposite ends of a single diameter. The shaker was driven by the amplified sinusoidal output of a signal generator. Before performing the frequency sweep, $L$ was inferred from the difference between the depth of the cup and the depth to the surface of the compacted granular medium. With this information the sample density is given by $\rho = M_0/(\pi R^2 L)$, where $M_0$ is the static mass of the granular media. The effective mass $\tilde{M}(f)$ was determined from the simultaneous measurement of the force, $\tilde{F}(f)$, and the acceleration, $\tilde{a}(f)$,

*Permanent address: School of Engineering, Brown University, Providence, RI 02906, USA; david_henann@brown.edu

 

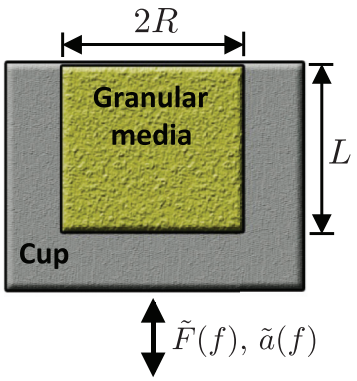


FIG. 1. (Color online) Schematic cross section of the cylindrical cup apparatus.

at the bottom of the cylindrical cup [see Eq. (1)], where $\tilde{a}(f)$ was determined by averaging that measured at the two points on opposite ends of the cup diameter. The measurements were performed at roughly 1200 evenly spaced discrete frequencies over a relatively broad band, $f = 0.1$–$8$ kHz. The magnitudes of $\tilde{F}(f)$ and $\tilde{a}(f)$ were measured with a lock-in amplifier, where the frequency of the shaker driving signal is the reference. Both of these quantities exhibited a phase shift with respect to the shaker drive, confirming that they are complex-valued and, consequently, that the effective mass is also a complex-valued quantity. We represent the real part of the effective mass as $M_1(f)$ and the imaginary part as $M_2(f)$. The real and imaginary effective mass for tungsten grains subjected to the mechanical compaction protocol are shown as solid lines in Figs. 2(a) and 2(b), respectively, for aspect ratios $R/L = 0.71$, 1.05, and 2.01, demonstrating that the ratios of resonant peaks for a given aspect ratio are not $1:3:5:7:\ldots$. The utility of these quantities for predicting the effect of a granular load on the broadband acoustic response of a resonant structure has been previously demonstrated [11,13].

### B. Mode-shape measurement

To gather information on the mode shapes at resonance [14], we employed a laser vibrometer to experimentally measure the complex-valued displacement, $\tilde{u}(i,j)$, at discrete points $(i,j)$ on the free surface of the granular medium at fixed frequencies. The laser was mounted on a right-angle bracket, attached to two translational stages. The position of each stage was controlled by a step motor, capable of translating each stage in perpendicular directions. At each position $(i,j)$ on the top surface of the granular medium, the velocity, $\tilde{v}(i,j) = \tilde{u}(i,j)(2\pi f)$, was determined from the doppler shift of the light reflected off of the granular medium. The magnitude of the velocity was measured with a lock-in amplifier, with the frequency of the shaker driving signal as the reference. After locating the center of the cup, the laser was systematically translated along the surface of the granular medium. These experiments were performed with a 25.4-mm-diameter cup, employing a step size of 0.5 mm. The spot size of the laser was on the order of $\sim$1 mm, so we characterize the mode shape at several locations as specified through a square two-dimensional array that has 48 elements per side. The indices $i,j = 1,2,3,\ldots,48$ represent the position of each

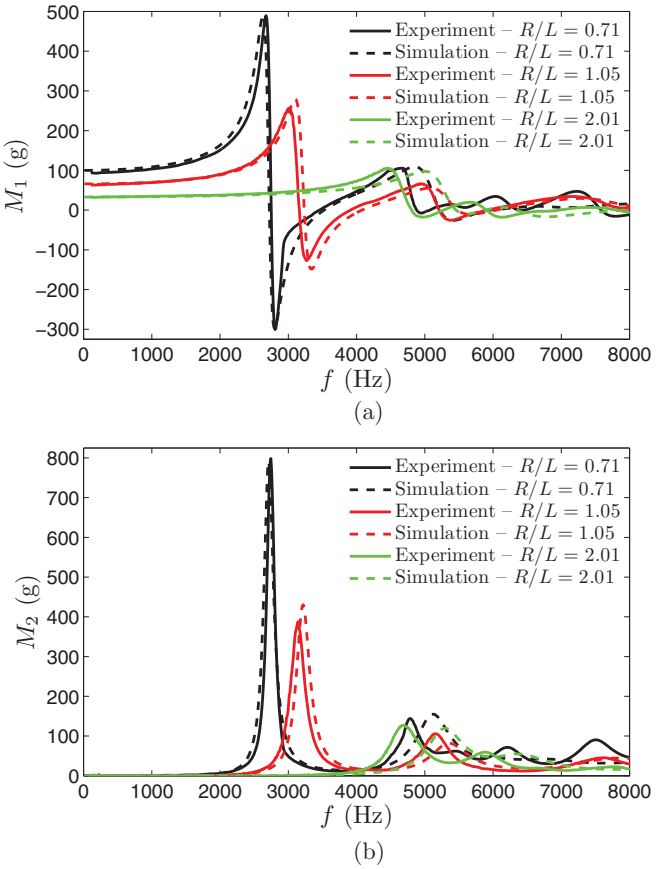


FIG. 2. (Color online) The (a) real $M_1$ and (b) imaginary $M_2$ effective mass spectra for several aspect ratios, $R/L = 0.71$ (black lines), 1.05 [red (gray)], and 2.01 [green (light gray)]. Solid lines represent experimental measurements while dashed lines are simulation results.

measurement in both dimensions. We did not take data at those points in the square array that correspond to locations outside of the cylindrical cup. At the same time, we monitored the acceleration at the bottom of the cup, $\tilde{a}_C(i,j)$. The magnitude of this value was also determined with a lock-in amplifier with the shaker driving signal as the reference. Assuming the cup is rigid, the displacement amplitude of the cup is given by $\tilde{u}_C(i,j) = \tilde{a}_C(i,j)/(2\pi f)^2$. The purpose of measuring the cup displacement is twofold. First, we want to ensure that the motion of the cup is uniform so that the displacement of the cup is a constant value, $\tilde{u}_C$, at each position $(i,j)$. Second, we utilize $\tilde{u}_C$ to normalize the displacement magnitude at each point on the free surface of the granular medium to determine the relative displacement between the granular medium and the cup, defined as

$$U_{\mathrm{rel}}(i,j) = \frac{|\tilde{u}(i,j)|}{|\tilde{u}_C|} - 1. \qquad (2)$$

Figures 3(a) and 3(b) show intensity plots for the normalized displacement field, $U_{\mathrm{rel}}(i,j)$, of the two lowest frequency resonant modes ($f_0 = 2740$ Hz and $f_1 = 4785$ Hz) for mechanically compacted tungsten grains and an aspect ratio of $R/L = 0.71$ (solid black lines in Fig. 2). Figures 3(a) and 3(b) demonstrate approximately axisymmetric mode shapes. Therefore, we compute the average value of $U_{\mathrm{rel}}$ at each

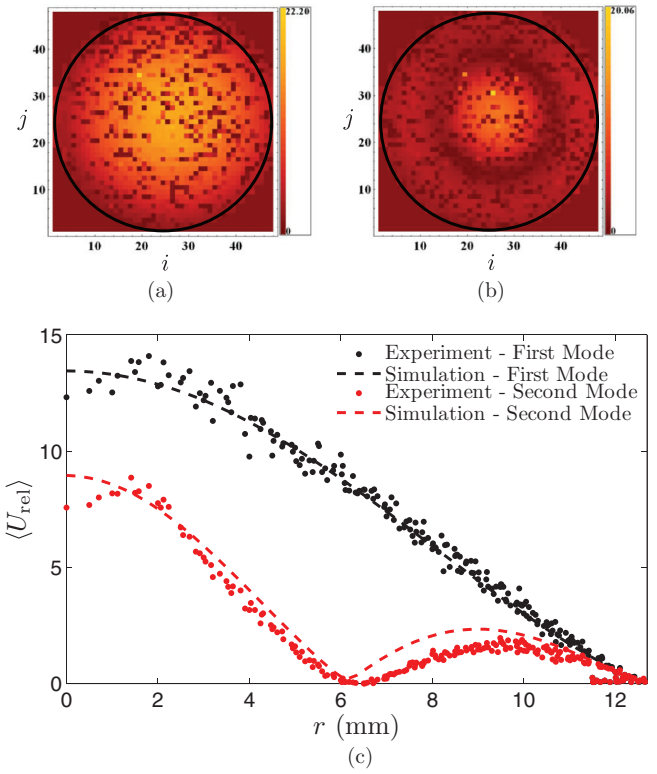


FIG. 3. (Color online) (a,b) Intensity plots from the laser vibrometer measurements showing the normalized displacement field, $U_{\rm rel}(i,j)$, of the two lowest frequency modes ($f_0 = 2740$ Hz and $f_1 = 4785$ Hz) corresponding to the $\tilde{M}(f)$ shown in Fig. 2 ($R/L = 0.71$). The black circular outlines indicate the perimeter of the cup. (c) The radial average of the relative displacement fields, along with that predicted by the finite-element model.

radial point $r$ (measured from the central axis of the cup) and denote this quantity by $\langle U_{\rm rel}\rangle$. This average relative displacement is plotted in Fig. 3(c) for the first two resonant peaks [black and red (gray) points, respectively]. Figure 3(c) allows for two important observations: (i) the mode shape is smooth, indicating continuum behavior, and (ii) the relative displacement is zero at the wall, indicating a no-slip wall condition.

In light of (ii), at a physical level we recognize that the grain-wall interaction is more precisely dictated by Coulombic friction, a nonlinear boundary condition. Our explanation for why this reduces to an effectively no-slip condition in actual realizations of granular packings hinges on the smallness of the vibration amplitudes. Noting that inertial forces on the grains decrease with the vibration amplitude, as amplitudes become small enough, the material tractions at the wall can be brought well beneath the wall's frictional resistance, precluding wall slip. We have verified this explanation with additional simulations. Using the commercial finite-element package ABAQUS/EXPLICIT [15], we performed simulations utilizing frictional boundary conditions in the configuration described above and observed the related assertion that for fixed, small-amplitude driving the no-slip condition is observed along the walls' entirety for typical wall friction coefficients. Recognizing our experiments are in this regime allows us to make the no-slip idealization, opening the door for linear modeling.

## III. SIMULATIONS

As is demonstrated in the following, accounting for the no-slip wall condition is crucial to rationalize the observed experimental results. In fact, we find that excellent agreement may be achieved by using a three-dimensional version of the Kelvin-Voigt viscoelastic constitutive model, in which the stress tensor $\boldsymbol{\sigma}$ is given as the sum of linear elastic and linear viscous parts: $\boldsymbol{\sigma} = \boldsymbol{\sigma}^{\rm e} + \boldsymbol{\sigma}^{\rm v}$. The elastic contribution is given by the familiar linear elastic relation

$$\boldsymbol{\sigma}^{\rm e} = \frac{E}{1+\nu}\boldsymbol{\epsilon} + \frac{E\nu}{(1+\nu)(1-2\nu)}(\mathrm{tr}\,\boldsymbol{\epsilon})\mathbf{1}, \tag{3}$$

where $\boldsymbol{\epsilon}$ is the infinitesimal strain tensor, $E$ is Young's modulus, and $\nu$ is Poisson's ratio. For the viscous part, we assume Rayleigh proportional stiffness damping, in which the viscous stress is simply given by

$$\boldsymbol{\sigma}^{\rm v} = \beta\left[\frac{E}{1+\nu}\dot{\boldsymbol{\epsilon}} + \frac{E\nu}{(1+\nu)(1-2\nu)}(\mathrm{tr}\,\dot{\boldsymbol{\epsilon}})\mathbf{1}\right], \tag{4}$$

where $\dot{\boldsymbol{\epsilon}}$ is the strain-rate tensor and $\beta$ is the Rayleigh stiffness damping parameter, having units of time. This model relies upon three material parameters, $E$, $\nu$, and $\beta$, to fully describe the dynamic response of the material. We understand the intrinsic limitation of a linear model with constant material parameters—as vibrational amplitudes get larger the nonlinear Hertzian interactions between grains becomes important [16]. However, we show that a linear constitutive model becomes an acceptable simplification for the purpose of general modeling of small-amplitude acoustics in bulk, dense-packed grains. Moreover, despite the well-known Hertzian contact mechanics of particles [17,18], we have verified in separate numerical calculations that nonlinear constitutive models based on Hertzian contacts (i.e., Jiang-Liu elasticity [9,10]) yield negligible improvement over the strictly linear constitutive model we use here.

### A. Effective mass

In order to predict the frequency spectrum of the effective mass, we perform finite-element calculations, utilizing the direct-solution steady-state dynamics analysis procedure in ABAQUS/STANDARD [15]. This linear solution technique calculates the complex-valued, steady-state response of a discretized system under harmonic excitation at a given frequency, $f$. The initial mesh configuration for an aspect ratio of $R/L = 0.71$ is shown in Fig. 4, and a similar mesh resolution is used for other aspect ratios. We make an axisymmetric simplification, with the axis of symmetry denoted in the figure. The nodes on the bottom and right-hand side of the mesh represent the granular material in contact with the cup floor and wall. In line with the observation of no slip at the wall, we apply the base excitation, i.e., the motion of the cup, directly to these nodes, using displacement control. The complex-valued reaction force is then determined from the simulation results at each frequency, allowing for the calculation of the effective mass spectra via Eq. (1). Since we have chosen a linear elastic constitutive

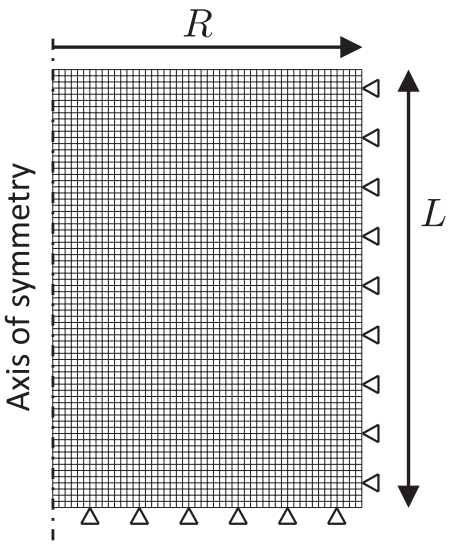


FIG. 4. Initial finite-mesh configuration for axisymmetric effective mass simulation ($R/L = 0.71$).

model, gravity has no effect on the simulated results and is therefore omitted.

Figure 2 shows an example of model calculations (dashed lines) for three of the various aspect ratios employed experimentally. For these calculations the Young's modulus of the mechanically compacted tungsten grains is taken to be $E = 162$ MPa. This value provides the best fit for the frequency of the first resonant peak $f_0$ for the three aspect ratios shown. The value of Poisson's ratio has little effect on the first resonant peak but does affect the location of the second peak $f_1$. A value of $\nu = 0.1$ was chosen to best fit this second peak in all cases. Finally, a single value of $\beta = 3.7 \times 10^{-6}$ s was taken to best fit the heights of the resonant peaks $f_0$ and $f_1$ in Fig. 2(b). The simple linear material model having only three material parameters does a good job of capturing the salient features of the effective mass spectra for the broad range of aspect ratio employed experimentally.

### B. Mode shapes

The model results also well describe the mode shapes of the first two resonant peaks. Figure 5 shows the calculated complex-valued displacement fields for the first two resonant peaks ($f_0 = 2711$ Hz and $f_1 = 5115$ Hz in the simulations) for $R/L = 0.71$. Half of the cylinder is displayed for clarity. Since the displacement field is complex valued, it may be parametrized by a phase angle, ranging from 0 to $2\pi$ rad. The displacement fields at $\pi/2$ and $3\pi/2$ rad are shown in Figs. 5(a) and 5(b), respectively, for the first resonant peak, while the same results are shown in Figs. 5(c) and 5(d) for the second resonant peak. (Movies of the full cycles are included in the Supplemental Material [19].) At these two points during the steady-state cycle, the displacement magnitudes in the bulk are at their maximum, and the displacements for phase angles of $\pi/2$ and $3\pi/2$ rad are negatives of each other. As expected for driving near resonance, the displacements in the bulk are out of phase with the cup motion, which attains maximums in magnitude at phase angles of 0 and $\pi$ rad. From these simulation results, we calculate the radial profile

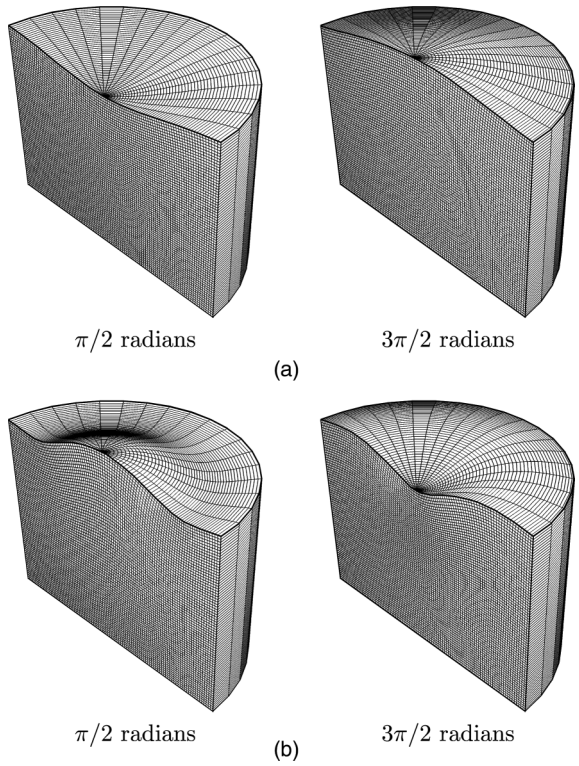


FIG. 5. (a) The simulated displacement fields for the first resonant peak ($f_0 = 2711$ Hz) at phase angles of $\pi/2$ and $3\pi/2$ rad for $R/L = 0.71$. (b) The same simulation result for the second resonant peak ($f_1 = 5115$ Hz) at phase angles of $\pi/2$ and $3\pi/2$ rad for $R/L = 0.71$.

of the average relative displacement on the top surface for $R/L = 0.71$ via Eq. (2) and plot the profiles for the first two resonant peaks using dashed lines in Fig. 3(c). The comparison to the experiments is excellent.

### C. Generalization to other granular systems

To this point, we have shown that our simple model is predictive for a single granular system and several aspect ratios. To demonstrate that our approach is general, we consider different preparation protocols, grain materials, and a wider range of aspect ratios. As the most important feature of the effective mass spectrum, we consider the frequency of the first resonant peak $f_0$ and its dependence upon the model geometry ($R$ and $L$) and material and preparation protocol ($\rho$, $E$, and $\nu$). (For the lightly damped case, i.e., small $\beta$, the numerical value of $\beta$ has a negligible effect on $f_0$ [20].) Using dimensional analysis, the functional dependence should be of the form

$$\frac{f_0 L}{\sqrt{E/\rho}} = g\left(\frac{R}{L}, \nu\right). \tag{5}$$

It is straightforward to probe this functional dependence using our simulation capability. We find that the function $g$ is insensitive to Poisson's ratio in a range from 0.0 to 0.2 and plot the normalized frequency $f_0 L/\sqrt{E/\rho}$ as a function of the aspect ratio $R/L$ as a solid line in Fig. 6 for $\nu = 0.1$.

We consider several consolidation protocols for the tungsten grains, achieving different degrees of compaction and thus

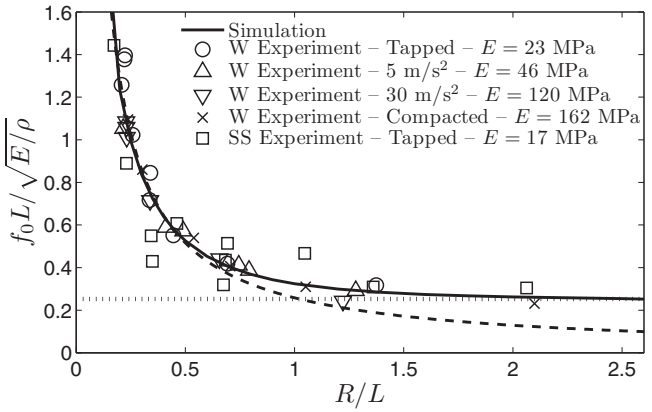


FIG. 6. Normalized frequency corresponding to $f_0$ (data points) from effective mass measurements with two metallic granular systems after a variety of handling protocols as a function of aspect ratio. The one notable free parameter, $E$, used to normalize the independent data sets is noted in the legend. Also shown is the prediction of linear finite-element simulations (solid line). Theoretical high and low aspect ratio limits are plotted as dotted and dashed lines, respectively.

acoustic properties. The lowest consolidation was achieved by simply tapping the side of the cylindrical cup, while slightly greater compaction was achieved by vibrating the granular medium at $f = 1$ kHz and $a = 5$ m/s$^2$. The latter protocol was also employed with a higher acceleration amplitude, $a = 30$ m/s$^2$, to achieve greater consolidation, and the greatest degree of consolidation was achieved with the aforementioned compaction protocol. While the mechanically compacted grains were coated with PDMS, all other samples were tested without coating. We also consider a stainless steel (SS) granular material with fairly spherical, monodisperse particles ($\sim 10^{-1}$ mm), subjected to tapping. While the aspect ratios for all tungsten samples were varied by changing the filling height with a fixed 25.4-mm-diameter cup, the cup radius was also varied for the SS samples, using cups with one of the following diameters (in mm): 6.35, 12.7, 25.4, or 37.5. The symbols in Fig. 6 show a compilation of the data for the normalized lowest frequency mode as a function of aspect ratio for each of the five granular systems described. To perform the normalization for each system, a value of the Young's modulus $E$ must be chosen. The value of $E$ used in the normalization process is noted in the legend for each granular system. The values of $E$ determined in this way are reasonable and follow the trend of increasing stiffness with greater compaction [11]. Once this free parameter is determined, the simulation well describes the effect of aspect ratio for all granular systems, providing further confidence that the simple linear model is physically representative of the behavior of the bulk granular media.

The high and low aspect ratio limits of the simulation may be understood using simple toy models. In the limit of $R/L \to \infty$, i.e., an infinitely wide cup, in which the walls have no effect, we recover the one-dimensional plane-wave response. In this case, due to the closed bottom and open top of the cup, the first resonant peak corresponds to a quarter wavelength longitudinal wave, expressed for a linear elastic material as $f_0 L/v_l = 0.25$, where $v_l$ is the longitudinal wave speed. Expressed in terms of the elastic material parameters, we have

$$\frac{f_0 L}{\sqrt{E/\rho}} = 0.25\sqrt{\frac{(1-\nu)}{(1+\nu)(1-2\nu)}}. \tag{6}$$

In the opposite limit of $R/L \to 0$, i.e., an infinitely tall cup, the displacements may be idealized as varying only with radial position and not vertical position, effectively ignoring end effects. Vibrational modes in this case correspond to that of a circular drum head with displacement increments along the direction of the cylinder axis, the lowest frequency mode being given by $2\pi f_0 R/v_t = 2.4$, where $v_t$ is the tangential wave speed and 2.4 arises as the first root of the zeroth-order Bessel function of the first kind. In terms of $E$ and $\nu$, the expression becomes

$$\frac{f_0 L}{\sqrt{E/\rho}} = \frac{2.4}{2\pi(R/L)\sqrt{2(1+\nu)}}. \tag{7}$$

For both cases, the dependence on the Poisson's ratio is weak in the range of 0.0 to 0.2. We plot the $R/L \to \infty$ limit [Eq. (6)] as a dotted line and the $R/L \to 0$ limit [Eq. (7)] as a dashed line in Fig. 6 for $\nu = 0.1$. In both cases, the limits are well described by the simple toy models, giving a sense of the underlying physics.

## IV. CONCLUSION

In closing, we recall that the results reported here are limited to (i) small-amplitude acoustics in (ii) densely packed matter. Regarding the first condition, small-amplitude excitations are crucial to achieving the effective no-slip wall interaction and linear material behavior, opening the door for the linear modeling approach pursued here. As larger amplitude excitations are considered, more complex, nonlinear frictional wall interactions as well as a nonlinear elastic material model, such as the Jiang-Liu model [9], may need to be included. Regarding the second condition, as we leave the dense-packed regime toward looser packings, we expect the predictive capability across the entire effective mass spectrum to lessen. However, the dominating behavior, i.e., the details of the lowest frequency mode, appear to be well captured over an array of consolidation levels (see Fig. 6). Under these two conditions, we have shown that a simple linear constitutive model is representative of the dynamic response of a dense-packed granular media, providing an excellent quantitative description of the effect of geometry on the effective mass spectra as well as the resonant mode shapes. The simulation capability works for various materials and preparations, and we expect the capability to be amenable to changes in geometry or other conditions, such as the application of a confining pressure to the top surface [20].

## ACKNOWLEDGMENTS

D.L.H. and K.K. acknowledge support from Schlumberger-Doll Research. Larry McGowan is gratefully acknowledged for assistance with experiments.

[1] C. Daraio, V. F. Nesterenko, E. B. Herbold, and S. Jin, Phys. Rev. E **72**, 016603 (2005).
[2] C. Daraio and V. F. Nesterenko, Phys. Rev. E **73**, 026612 (2006).
[3] C. Daraio, V. F. Nesterenko, E. B. Herbold, and S. Jin, Phys. Rev. E **73**, 026610 (2006).
[4] W. Kuhl and H. Kaiser, Acustica **2**, 179 (1962).
[5] L. Cremer and M. Heckl, *Structure Borne Sound* (Springer, Berlin, 1973).
[6] J. M. Bourinet and D. Le Houedec, in *Powders & Grains*, edited by R. Behringer and J. Jenkins (Balkema, Rotterdam, 1997), Vol. 97.
[7] J. C. Sun, H. B. Sun, L. C. Chow, and E. J. Richards, J. Sound Vib. **104**, 243 (1986).
[8] S. A. Nayfeh, J. M. Verdirame, and K. K. Varanasi, Proc. SPIE **4697**, 158 (2002).
[9] Y. Jiang and M. Liu, Phys. Rev. Lett. **91**, 144301 (2003).
[10] L. Bonneau, B. Andreotti, and E. Clement, Phys. Rev. E **75**, 016602 (2007).
[11] J. Valenza, C.-J. Hsu, R. Ingale, N. Gland, H. A. Makse, and D. L. Johnson, Phys. Rev. E **80**, 051304 (2009).
[12] J. J. Valenza and D. L. Johnson, Phys. Rev. E **85**, 041302 (2012).
[13] J. J. Valenza, C.-J. Hsu, and D. L. Johnson, J. Acoust. Soc. Am. **128**, 2768 (2010).
[14] Regarding our "resonance" terminology, we drive the system at a frequency equal to the real part of the complex-valued normal mode frequency, which has the effect of maximizing the contribution of the mode in question to the observed displacement field.
[15] ABAQUS, reference manuals, 2010.
[16] L. R. Gómez, A. M. Turner, M. van Hecke, and V. Vitelli, Phys. Rev. Lett. **108**, 058001 (2012).
[17] K. L. Johnson, *Contact Mechanics* (Cambridge University Press, Cambridge, UK, 1985).
[18] H. A. Makse, N. Gland, D. L. Johnson, and L. Schwartz, Phys. Rev. E **70**, 061302 (2004).
[19] See Supplemental Material at http://link.aps.org/supplemental/10.1103/PhysRevE.88.042205 for full-cycle movies of the first two resonant modes for $R/L = 0.71$.
[20] Y. Hu, D. L. Johnson, J. J. Valenza, and H. A. Makse (unpublished).